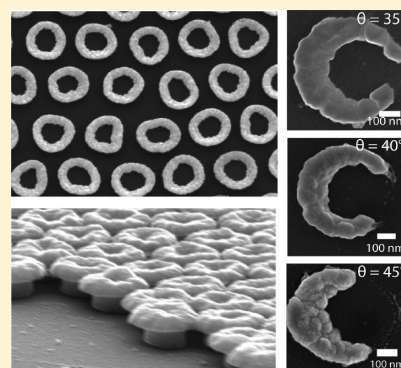


# Lithographically Patterned Nanoscale Electrodeposition of Plasmonic, Bimetallic, Semiconductor, Magnetic, and Polymer Nanoring Arrays

Kyunghee Cho, Gabriel Loget, and Robert M. Corn\*

Department of Chemistry, University of California—Irvine, Irvine, California 92697, United States

**ABSTRACT:** Large area arrays of magnetic, semiconducting, and insulating nanorings were created by coupling colloidal lithography with nanoscale electrodeposition. This versatile nanoscale fabrication process allows for the independent tuning of the spacing, diameter, and width of the nanorings with typical values of 1.0  $\mu\text{m}$ , 750 nm, and 100 nm, respectively, and was used to form nanorings from a host of materials: Ni, Co, bimetallic Ni/Au, CdSe, and polydopamine. These nanoring arrays have potential applications in memory storage, optical materials, and biosensing. A modified version of this nanoscale electrodeposition process was also used to create arrays of split gold nanorings. The size of the split nanoring opening was controlled by the angle of photoresist exposure during the fabrication process and could be varied from 50% down to 10% of the ring circumference. The large area ( $\text{cm}^2$  scale) gold split nanoring array surfaces exhibited strong polarization-dependent plasmonic absorption bands for wavelengths from 1 to 5  $\mu\text{m}$ . Plasmonic nanoscale split ring arrays are potentially useful as tunable dichroic materials throughout the infrared and near-infrared spectral regions.



## 1. INTRODUCTION

The unique physical properties attributed to nanoscale materials have led to a rise of nanomaterials research in recent years. For example, nanopatterned magnetic structures have been studied for applications as varied as high-density data storage to biomedical sensing.<sup>1–4</sup> Semiconducting nanostructures have been developed for quantum confined materials and devices.<sup>5–7</sup> Additionally, plasmonic nanomaterials have received much attention due to their unique optical and electronic properties as well as their potential implementation in a variety of applications including ultrasensitive biosensors, enhanced surface-sensitive spectroscopy, and optical metamaterials.<sup>8–14</sup> Optical metamaterials, defined as periodic structures whose features are smaller than the wavelength of light, can be used to create a variety of unique optical effects: negative refractive index materials, cloaking devices, and perfect lenses.<sup>11,15</sup>

The fabrication of nanoring arrays has been of particular interest in nanomaterials research. Magnetic nanorings have been proposed as an ideal candidate for use in random access memory devices due to their well-defined magnetic remnant states, which would be suitable for data storage of multiple bits for each ring.<sup>1,16</sup> Also, the strong plasmonic resonance arising from gold nanorings has been used for detecting polymer film growth and for DNA biosensing.<sup>10</sup> In addition to nanorings, an optical metamaterial that has been the focus of much interest is arrays of split ring resonators, which have been exploited to create materials with negative permeability and negative refractive index in the near-infrared (NIR), infrared (IR), and microwave spectral regions.<sup>17–19</sup> Plasmonic split nanoring arrays exhibit a strongly polarization-dependent absorption spectrum and can be employed for nanophotonic biosensors

and plasmonic NIR dichroic polarizing filters.<sup>12,20</sup> In addition, electromagnetic hot spots in the closely related nanocrescent structures have been used in localized surface plasmon resonance based sensing and surface-enhanced spectroscopies (e.g., Raman and infrared absorption).<sup>21–25</sup> Composite plasmonic and magnetic nanocrescents have been employed as surface-enhanced Raman scattering substrates that are capable of being controlled by external magnetic fields.<sup>26</sup>

This recent growth in nanotechnology has necessitated the development of facile, inexpensive, and high-throughput processes for the fabrication of nanoscale periodic arrays that are made of a large number of materials. While electron beam lithography (EBL) can be used to generate such nanostructures on the scale of tens to hundreds of microns,<sup>12,18,20,27,28</sup> the time and cost required to fabricate arrays over larger areas using EBL is prohibitive. Alternatively, patterned nanostructures have been fabricated using such methods as nanochannel glass replica membranes,<sup>29,30</sup> colloidal lithography,<sup>31</sup> and evaporative self-assembly.<sup>32</sup> We have recently described a novel method for the fabrication of plasmonic nanoring arrays over large areas ( $\text{cm}^2$ ) that combines colloidal lithography with lithographically patterned nanoscale electrodeposition (LPNE).<sup>33</sup>

In this paper, we expand the use of this nanofabrication method to make large-scale arrays of nanorings and split nanorings from a wide range of materials, including magnetic

**Special Issue:** John C. Hemminger Festschrift

**Received:** February 19, 2014

**Revised:** June 16, 2014

**Published:** June 17, 2014

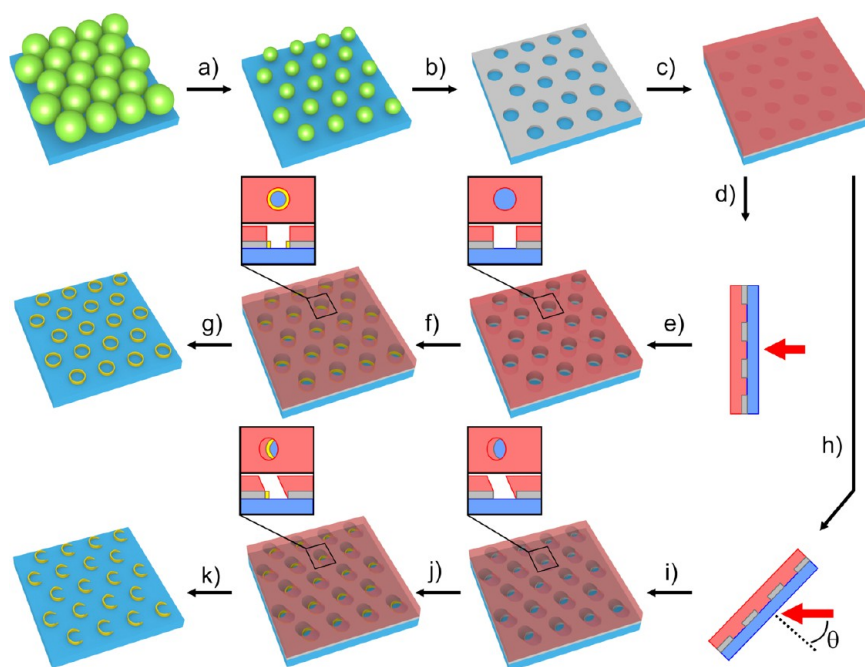


**Figure 1.** Nanoring and split nanoring array fabrication scheme: (a) polystyrene beads self-assembled in a monolayer are etched to size in an oxygen plasma; (b) nanohole mask is formed by vapor depositing silver over the etched beads and removing the beads; (c) positive photoresist is spin coated onto the nanohole mask. For nanorings: (d) photoresist is backside exposed at normal incidence through the nanoholes; (e) holes are formed in the photoresist upon development; (f) nanorings are electrodeposited onto the exposed silver; and (g) photoresist and silver are removed to reveal nanorings. For split nanorings: (h) exposure at an angle  $\theta$  leaves part of the nanohole covered by photoresist after (i) development; (j) split nanoring is electrodeposited through the holes formed in the photoresist to the exposed silver; and (k) split nanorings arrays are completed upon photoresist and silver removal.

materials (nickel and cobalt), semiconductors (cadmium selenide), and insulating polymers (polydopamine). Additionally, we present bimetallic (nickel/gold) and split gold nanoring arrays as examples of extending our fabrication strategy to create more complex nanostructured surfaces. The large area fabrication method described here provides a high degree of control over nanoscale features such as spacing, radii, thickness, and (in the case of split nanorings) the ring opening size.

## 2. EXPERIMENTAL SECTION

**2.1. Materials.** Carboxylate-coated polystyrene bead solutions (2.6% w/v, 1  $\mu\text{m}$  diameter) were purchased from Polysciences (Warrington, PA). Shipley S1808 photoresist, Thinner P, and MF-319 developer were purchased from Microchem (Newton, MA). Clean Earth Chemicals 24K gold plating solution (Grobet USA, Carlstadt, NJ) was used as received. Fisher Premium glass microscope slides (1 mm thick) were used as substrates. Magnetite nanoparticles of 20 nm (20 mg/mL in citrate buffer) were purchased from nanoComposix (San Diego, CA) and diluted 1000-fold in water prior to use.

**2.2. Nanoring and Split Nanoring Array Fabrication.** A densely packed monolayer of polystyrene beads was formed by spin coating polystyrene beads (concentrated to 5.2% in 3:1 methanol:water) on hydrophilic oxygen plasma cleaned microscope glass slides cut to 2.5 cm  $\times$  2.5 cm pieces. Upon drying, the beads were etched in oxygen plasma (200 mTorr, 50 W,  $-400$  VDC, South Bay Technologies, San Clemente, CA) for 5 min. A 70 nm layer of Ag (over a 1 nm Cr adhesion layer) was vapor deposited on top of the etched beads by thermal evaporation. To remove the beads, the samples were sonicated sequentially in toluene and acetone. Shipley S1808 photoresist (diluted 1:1 with Thinner P) was spin coated on the nanohole

arrays (80 s, 2500 rpm) and baked for 20 min at 90  $^{\circ}\text{C}$ . The photoresist was backside exposed through the nanohole array with 20 mW/cm<sup>2</sup>. For split nanoring arrays, the angle of exposure was controlled by mounting the samples onto triangular blocks cut to achieve the desired angles. A potentiostat (PGSTAT12, Metrohm, Riverview, FL) was used for electrodeposition. Ni, Co, CdSe, and Au were deposited by potentiostatic electrodeposition using the following plating conditions: Ni,  $-0.85$  V for 9 min using a Ni plating solution (5 mM NiCl<sub>2</sub>, 5 mM boric acid, 0.1 M KCl); Co,  $-1.2$  V for 2.5 min using a Co plating solution (0.14 M CoSO<sub>4</sub> and 0.65 M boric acid); CdSe,  $-0.64$  V for 7 min using a CdSe plating solution (0.30 M CdSO<sub>4</sub>, 0.70 mM SeO<sub>2</sub>, and 0.25 M H<sub>2</sub>SO<sub>4</sub>); Au,  $-0.85$  V for 10 min using a commercial gold plating solution. Polydopamine was deposited by cyclic voltammetry (20 scans at a rate of 20 mV/s; vertex potentials of  $-0.6$  and  $0.66$  V) in a dopamine solution (5 mM dopamine in phosphate buffer (pH 6.5)). All potentials were measured versus a Ag/AgCl reference electrode; a Pt foil was used as the counter-electrode. After electrodeposition, the photoresist was washed off with acetone. The Ag sacrificial electrode was removed with a 5% NH<sub>4</sub>OH and 1% H<sub>2</sub>O<sub>2</sub> etching solution.

**2.3. Sample Characterization.** SEM: The samples were imaged on a FEI Magellan scanning electron microscope. XRD: Grazing incidence X-ray diffraction measurements were performed on a Rigaku SmartLab X-ray Diffractometer. FT-NIR Absorption Spectra: A Mattson RS-1 FTIR with a halogen source, CaF<sub>2</sub> beamsplitter, and InSb detector was used to capture NIR spectra from 2000 to 10000 cm<sup>-1</sup>. The beam was focused to 3 mm in diameter to interrogate different areas of the sample. A bare glass slide was used as the background reference spectrum.

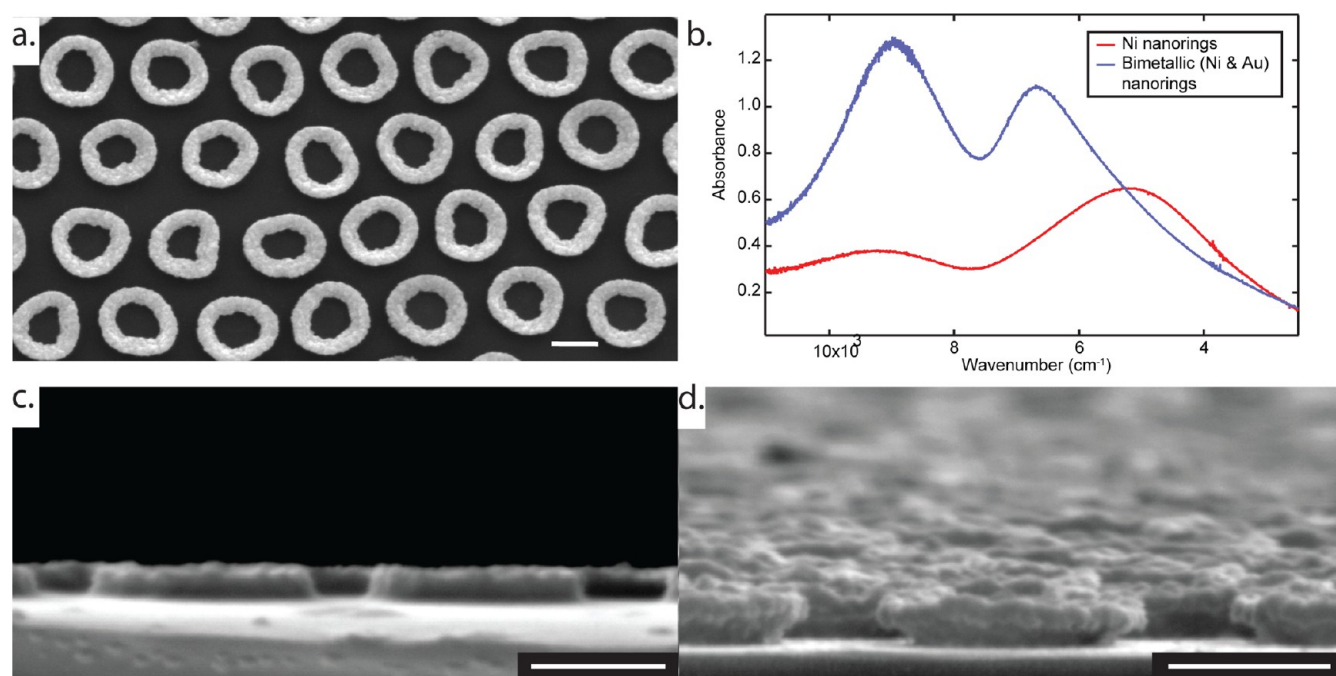


**Figure 2.** (a) Top-down SEM image of the nickel nanoring array. (b) FT-NIR absorbance spectra of nickel (red) and core-shell nickel/gold (blue) nanoring arrays. (c,d) Cross-sectional views of nickel/gold rings before (c) and after (d) etching of nickel in nitric acid. Scale bars: 500 nm.

### 3. RESULTS AND DISCUSSION

#### 3.1. Nanoring and Split Nanoring Array Fabrication.

Our method to fabricate magnetic, semiconducting, bimetallic, and insulating nanoring arrays and plasmonic split nanoring arrays (illustrated in Figure 1) is an extension of our previous methodology for lithographically patterned electrodeposition of plasmonic nanoring arrays.<sup>33</sup> First, carboxylate-functionalized polystyrene beads dispersed in a mixture of ethanol and water are spin-cast onto an oxygen plasma treated glass substrate to form a tightly packed monolayer. The beads are then etched to the desired size in oxygen plasma (Figure 1a). A sacrificial metal film (70 nm silver) is then formed by evaporation deposition over the etched beads, which are subsequently dissolved in toluene, yielding a nanohole array (Figure 1b). Positive photoresist is then spin coated over the nanohole array (Figure 1c). For closed nanoring fabrication, exposure of the photoresist at normal incidence (Figure 1d) results in complete opening of the nanoholes. In contrast, for split nanoring arrays, exposure at an angle  $\theta$  from the surface normal (Figure 1h) leaves part of the photoresist unexposed; thus, the holes do not completely open upon photoresist development (Figure 1i). During the electrodeposition step (Figure 1f and 1j), with the nanohole array acting as the working electrode, the desired material can only be deposited on the exposed metal. This process results in fully closed nanoring arrays when  $\theta = 0^\circ$  (Figure 1g) or split nanorings when exposed at an angle (Figure 1k) after removal of photoresist and sacrificial metal material.

This fabrication method combination offers complete control over all size parameters of the array. As discussed previously,<sup>33</sup> the periodicity of individual split nanorings is determined by the initial size of the polystyrene beads; the outer diameter is controlled by the time exposed to oxygen plasma; and the nanoring thickness and inner diameter are controlled by amount of charge passed during the electrodeposition process. Finally, the nanoring opening size is determined by the

exposure angle  $\theta$  ( $\theta = 0^\circ$  for closed rings). The described method produces square centimeter scale arrays of nanoscale structures while avoiding relatively expensive and time-consuming sequential fabrication processes such as EBL. In addition to size and dimensional control, we are able to form nanoring arrays from a broad range of materials available for electrodeposition.

**3.2. Magnetic Nanorings and Nanomushrooms.** Using our combined colloidal lithography and nanoscale electrodeposition process, we have fabricated nanoring arrays of nickel, a well-known ferromagnetic material. A top-down scanning electron microscope (SEM) image of a Ni nanoring array formed from 1  $\mu\text{m}$  diameter polystyrene beads is shown in Figure 2a. In addition to simply nickel nanorings, we have formed composite magnetic and plasmonic nanorings by sequential electrodeposition of nickel and gold (step “g” in Figure 1). By this process, the resulting bimetallic nanorings have a core of nickel and a shell of gold; the shell does not completely envelope the nickel because the outer part of the nickel rings is not available for gold electrodeposition. We confirmed this core-shell structure by etching away exposed nickel in nitric acid; when compared to the bimetallic structure before etching (Figure 2c), a distinct gold lip over where the nickel had been is visible (Figure 2d). Fourier transform near-infrared (FT-NIR) absorbance spectra of nickel and nickel/gold nanoring arrays are depicted in Figure 2b. The nickel spectrum shows a resonance at 5000  $\text{cm}^{-1}$  and a weaker higher-order resonance at 9000  $\text{cm}^{-1}$ . As expected, the addition of a gold shell greatly enhances the resonant response of the nanoring arrays. Interestingly, we see a strong and distinct double resonance for our bimetallic nanorings, which likely corresponds to two resonances from nickel and gold.

In addition to nickel, we have also fabricated magnetic nanostructures with cobalt. The cobalt deposition was performed by potentiostatic electrodeposition in an electrolyte containing cobalt sulfate and boric acid.<sup>34</sup> Successful deposition



of cobalt was confirmed by XRD (Figure 3d). While a top-down view (Figure 3a) of the cobalt structures makes the array

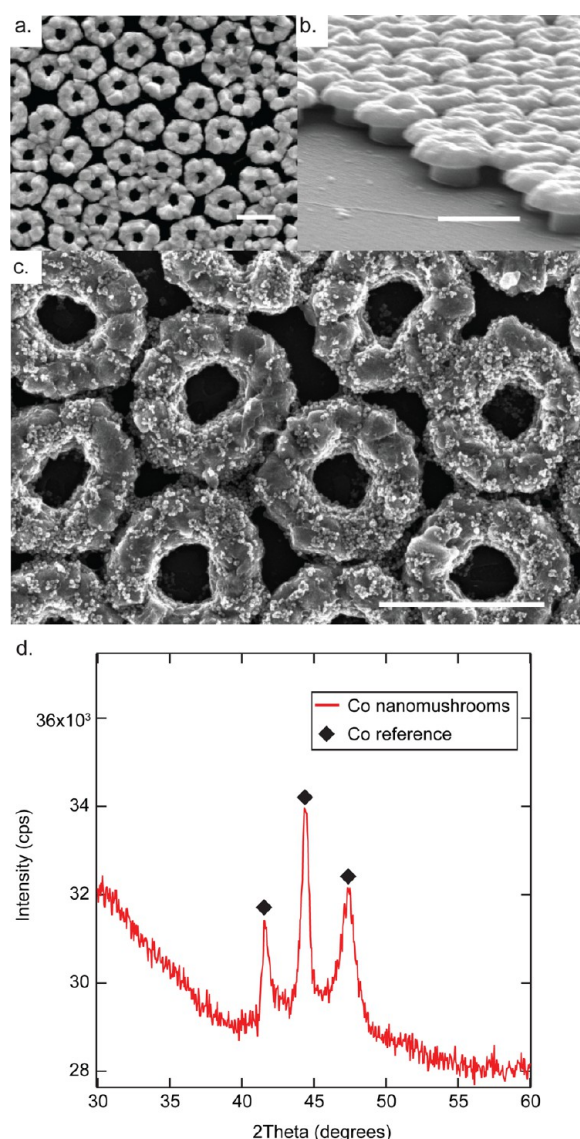


**Figure 3.** (a,b) Top-down (a) and tilted (b) SEM images of cobalt nanomushrooms. (c) Cobalt nanomushrooms after immersion in a solution of magnetite nanoparticles. (d) Confirmation by XRD of cobalt electrodeposition. Scale bars: 1  $\mu\text{m}$ .

appear as tightly packed rings, a tilted view (Figure 3b) on the SEM reveals mushroom-like structures. These “nanomushrooms” are a result of electrodeposition out of the photoresist hole to the top of the photoresist layer. We tested the ferromagnetism of the nanomushrooms by immersing the array into a solution of 20 nm magnetite nanoparticles. After thorough rinsing in water and ethanol, followed by drying under a nitrogen stream, the studding of the nanomushrooms by the nanoparticles was confirmed by SEM (Figure 3c). The physical anisotropy present in these nanomushrooms is difficult to replicate using traditional nanofabrication strategies and opens the door to facile production of similar structures made with magnetic or nonmagnetic materials.

**3.3. Semiconducting and Insulating Nanorings.** Along with metallic nanoring arrays, we are also able to fabricate nanorings of semiconducting and insulating materials. As an

example of nanoring arrays of a semiconductor material, we electrodeposited cadmium selenide by potentiostatic deposition (SEM image shown in Figure 4a) and confirmed the structure by XRD analysis (Figure 4b). Our fabrication method could provide a facile and high-throughput route for production of quantum rings.

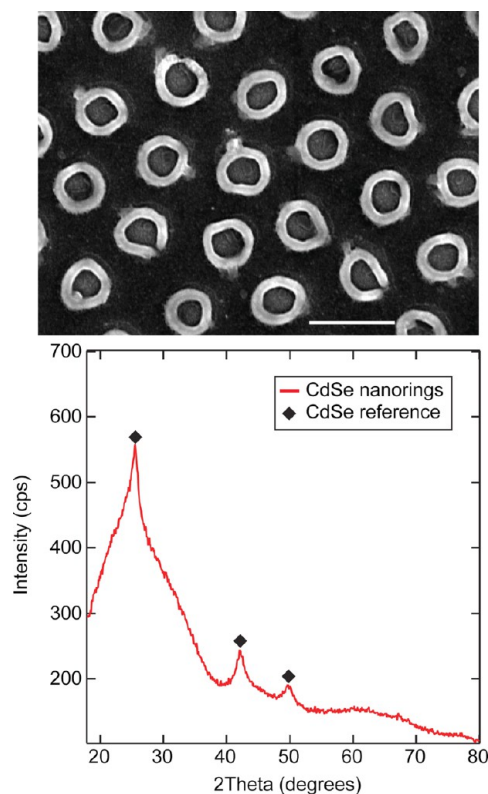


**Figure 4.** SEM image of CdSe nanorings and confirmation of CdSe electrodeposition by XRD. Scale bar: 1  $\mu\text{m}$ .

Additionally, nanoring arrays of insulating materials have been fabricated using this process. We have recently reported the electrodeposition of polydopamine (PDA) thin films for patterning DNA microarray.<sup>35</sup> This deposition was performed by repeated cyclic voltammetry (CV) scans at a carefully controlled pH. Our nanoring fabrication strategy allows us to scale down PDA electrodeposition to the nanoscale. Figure 5a depicts SEM images of PDA nanorings at two magnifications. While we expect the thickness of these PDA rings to be around 3 nm,<sup>35</sup> we can see in the inset that the thickness appears to be much greater, which we attribute to the collapsing of the PDA structure upon removal of the sacrificial electrode. As expected, the cathodic and anodic currents in the cyclic voltammograms decrease with repeated cycle numbers as the surface becomes more coated with PDA and thus electrically passivated. As we have shown previously with macroscale films, these nanoscale PDA ring arrays will allow the development of nanoscale biosensing platforms.

**3.4. Split Nanorings.** In addition to forming nanorings of a multitude of materials, our fabrication strategy allows us to also produce split nanorings and control the ring opening size. Gold split nanoring arrays were characterized by a combination of SEM and polarized Fourier transform near-infrared (FT-NIR) spectroscopy. As shown in the SEM image in Figure 6a, this angled photoexposure process creates an array where the

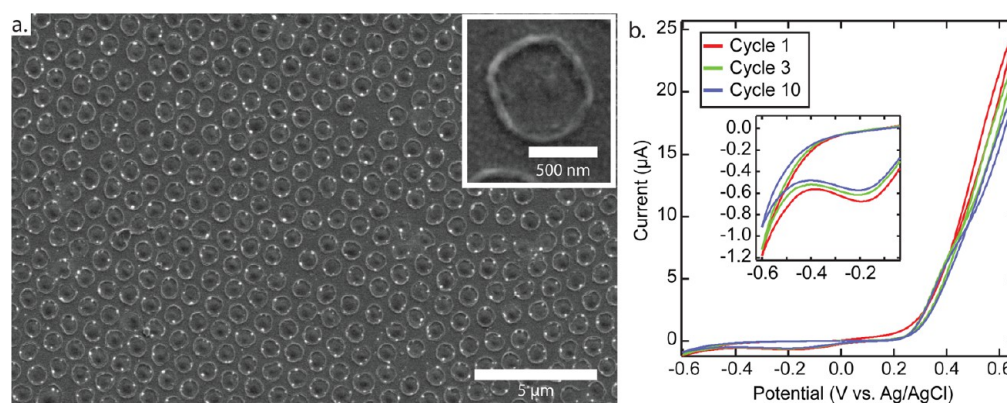


**Figure 5.** (a) SEM images of PDA nanorings at low and high (inset) magnifications. (b) Cyclic voltammograms of cycles 1, 3, and 10 during the growth of PDA nanorings.

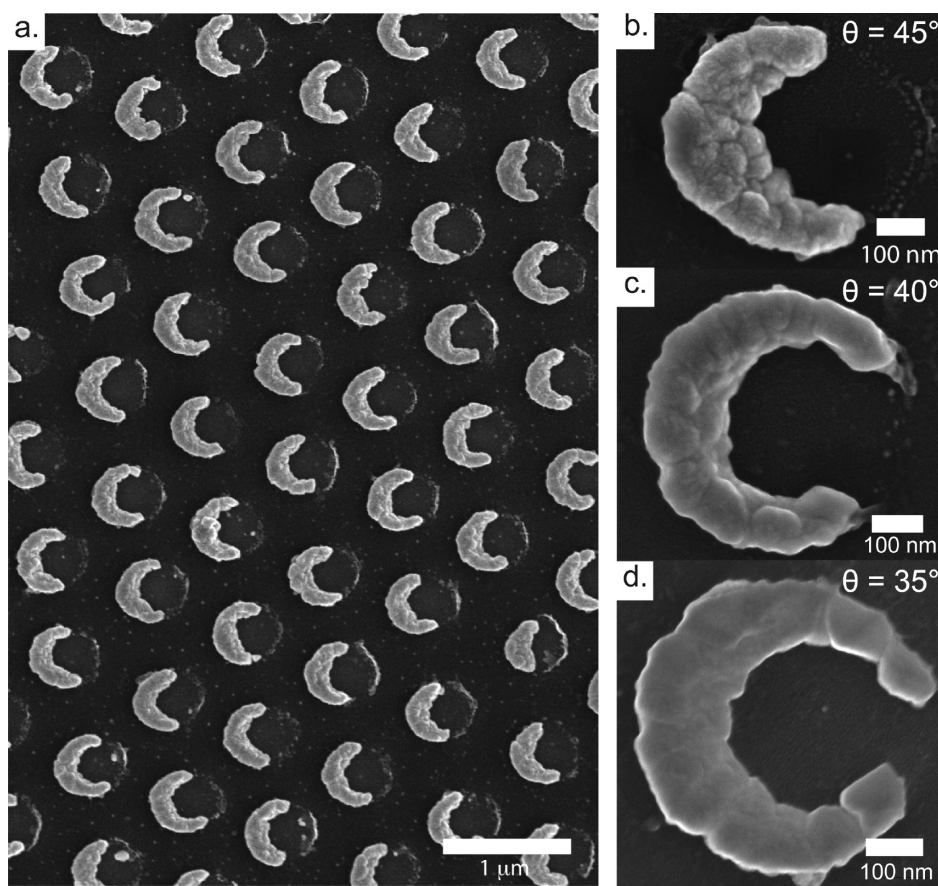


**Figure 6.** SEM images of nanocrescents and split nanorings. The size of the ring openings decreases with the angle of the backside UV exposure,  $\theta$ : (a) and (b)  $\theta = 45^\circ$ , (c)  $\theta = 40^\circ$ , and (d)  $\theta = 35^\circ$ .

openings are all on the same position on the nanorings. The size of the nanoring opening can be tuned by varying the exposure angle ( $\theta$ ) of the photoresist, as seen in the SEM images in Figures 6b–6d. For a given exposure dosage, a smaller  $\theta$  results in smaller ring openings. As seen in the SEM images, the ring opening can be controlled to be 50%, 20%, or 10% of the ring circumference by exposing at a  $\theta$  of  $45^\circ$ ,  $40^\circ$ , and  $35^\circ$ , respectively.

The NIR absorption spectra of these gold split nanoring arrays were characterized as a function of optical polarization with respect to the ring gap orientation. Transmission spectra were taken with light at normal incidence to the array surface.

In this configuration, the split ring arrays exhibit strong infrared resonances that are dependent on the polarization of the incident light. As seen in Figure 7, two distinct resonances are apparent in the near- to mid-infrared region as the polarization of the light is varied from  $\varphi = 0^\circ$  (perpendicular to the ring opening; red trace),  $\varphi = 30^\circ$  (orange trace),  $\varphi = 60^\circ$  (green trace), to  $\varphi = 90^\circ$  (blue trace). Two bands are observed in the optical spectrum: one at  $7400\text{ cm}^{-1}$  that dominates when  $\varphi = 0^\circ$  and the other at  $3800\text{ cm}^{-1}$  that dominates when  $\varphi = 90^\circ$ .

These two NIR bands are plasmonic resonances of split nanoring arrays that have been observed previously.<sup>27,28,36–38</sup> The openings in the nanorings break the symmetry of the ring



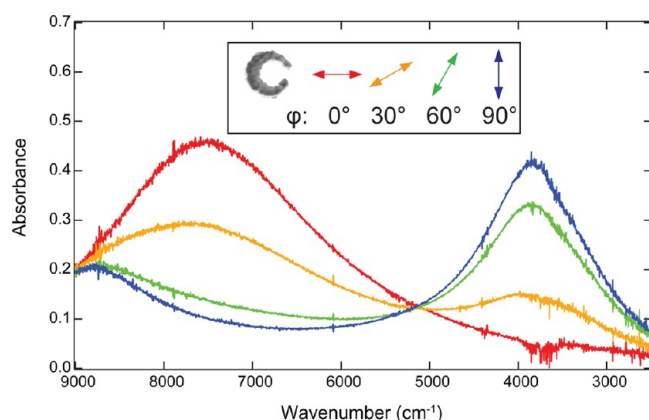


**Figure 7.** Polarization dependence of near-infrared absorbance for a split ring array. Polarization of the incident light was rotated in  $30^\circ$  increments on the same spot of the same sample starting perpendicular to the ring openings (red,  $\varphi = 0^\circ$ ) and continuing until parallel to the ring openings (blue,  $\varphi = 90^\circ$ ).

geometry and drastically change the surface charge distributions (and thus the optical responses) for different polarization states. The lower-frequency resonance in Figure 7 (at  $3800\text{ cm}^{-1}$ ) that dominates when light is polarized across the ring opening ( $\varphi = 90^\circ$ ) is commonly referred to as the LC resonance, in which the gap in the split ring acts as a capacitor. Following this analogy, decreased capacitance from larger gaps results in higher-frequency resonances. The higher-frequency resonance in Figure 7 (at  $7400\text{ cm}^{-1}$ ), which is strongest when light is polarized perpendicular to the ring opening ( $\varphi = 0^\circ$ ), corresponds to a plasmon mode that redshifts in response to smaller ring openings. As expected, the LC resonance becomes dampened as the polarization is rotated and less of the electric field is directed across the ring opening; this resonance disappears completely after  $90^\circ$  rotation.

The position of the two resonances could be controlled by varying the size of the rings and the amount of nanoring opening. Figure 8 depicts the responses to light polarization along (8a,  $\varphi = 0^\circ$ ) and across (8b,  $\varphi = 90^\circ$ ) the ring openings for the three samples imaged in Figure 6 formed with back exposure angle  $\theta = 45^\circ$  (blue trace),  $\theta = 40^\circ$  (green trace), and  $\theta = 35^\circ$  (red trace). As noted above, all conditions other than  $\theta$  were the same (i.e., the only difference between the three samples was the size of the ring openings). As the nanoring openings increase with increased exposure angle  $\theta$ , both the higher- and lower-frequency resonances (corresponding to the resonances for the two polarizations) appear at higher wavenumbers. The blueshift of the higher-frequency resonance with increasing ring opening in Figure 8a can be attributed to the decrease in the sides of the rings as the opening gets larger. The LC resonance (Figure 8b) also blueshifts with larger ring openings, as expected. For our split nanorings, the position of this LC resonance could be tuned to a range greater than  $2000\text{ cm}^{-1}$  by simply changing the size of the ring opening. For comparison, the peak resonance position of fully closed nanorings (fabricated under the same conditions with normal incidence exposure of the photoresist) is indicated by the dotted lines in Figure 8. Predictably, the resonance position for fully closed rings does not change with polarization.

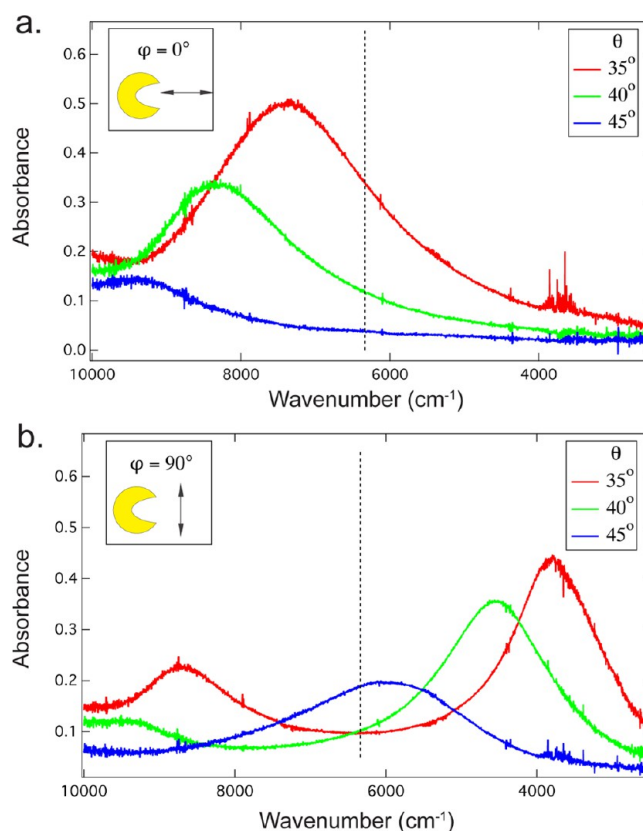


**Figure 8.** Effect of back exposure angle,  $\theta$  (i.e., ring opening size; same samples as depicted in Figure 6), on near-infrared absorbance for (a) polarization perpendicular to the opening and (b) polarization across the ring opening. The dotted line indicates the position of the polarization-independent plasmonic resonance for an array of fully closed rings.

#### 4. CONCLUSIONS

In summary, we have expanded the application of our method for fabricating densely packed and well-ordered nanoring arrays over large areas with a combination of colloidal lithography and LPNE to a variety of electrodeposited materials: magnetic (Ni and Co), semiconductor (CdSe), and insulator (PDA). Additionally, we have shown that this nanofabrication process can be modified to create unique asymmetric nanomushrooms, bimetallic core-shell nanorings, and split nanoring arrays. The plasmonic split gold nanoring arrays display polarization-dependent absorbances over a broad frequency range ( $8000\text{ cm}^{-1}$ ). By having complete control of the spacing, diameter, ring width, and gap size of these split ring resonators, we can tune the optical properties throughout the near-infrared and create dichroic materials in the spectral range from  $1$  to  $5\text{ }\mu\text{m}$ . In addition to their potential use as metamaterials, plasmonic split nanoring arrays can also be used as improved refractive index based biosensor surfaces for detecting nucleic acids and proteins.<sup>9,20,22,39</sup> In the future, split magnetic nanorings can also be created with this fabrication method; split magnetic nanorings have been used to stabilize and alter the magnetic flux closure states of magnetic nanorings with potential applications in high-density magnetic memory storage.<sup>40,41</sup>

#### AUTHOR INFORMATION

##### Corresponding Author

\*E-mail: rcorn@uci.edu.

## Notes

The authors declare no competing financial interest.

## ACKNOWLEDGMENTS

The authors thank Dr. Aaron Halpern and Jennifer B. Wood for helpful discussions. This work was supported by the NIH through grant R01-GM059622. SEM and XRD analyses were performed at the Laboratory for Electron and X-ray Instrumentation (LEXI) at UC Irvine.

## REFERENCES

- (1) Vaz, C. A. F.; Klaui, M.; Heyderman, L. J.; David, C.; Nolting, F.; Bland, J. A. C. Multiplicity of Magnetic Domain States in Circular Elements Probed by Photoemission Electron Microscopy. *Phys. Rev. B* **2005**, *72*, 224426.
- (2) Miller, M. M.; Prinz, G. A.; Cheng, S.-F.; Bounnak, S. Detection of a Micron-Sized Magnetic Sphere Using a Ring-Shaped Anisotropic Magnetoresistance-Based Sensor: A Model for a Magnetoresistance-Based Biosensor. *Appl. Phys. Lett.* **2002**, *81*, 2211–2213.
- (3) Klaui, M.; Vaz, C. A. F.; Bland, J. A. C.; Wernsdorfer, W.; Faini, G.; Cambril, E.; Heyderman, L. J. Domain Wall Motion Induced by Spin Polarized Currents in Ferromagnetic Ring Structures. *Appl. Phys. Lett.* **2003**, *83*, 105–107.
- (4) Tang, Z.; Kotov, N. A.; Giersig, M. Spontaneous Organization of Single CdTe Nanoparticles into Luminescent Nanowires. *Science* **2002**, *297*, 237–240.
- (5) Chen, P.; Chua, S. J.; Wang, Y. D.; Sander, M. D.; Fonstad, C. G. InGaN Nanorings and Nanodots by Selective Area Epitaxy. *Appl. Phys. Lett.* **2005**, *87*, 143111.
- (6) Tian, Y.; Sakr, M. R.; Kinder, J. M.; Liang, D.; MacDonald, M. J.; Qiu, R. J.; Gao, H.; Gao, X. P. A. One-Dimensional Quantum Confinement Effect Modulated Thermoelectric Properties in InAs Nanowires. *Nano Lett.* **2012**, *12*, 6492–6497.
- (7) Vayssieres, L.; Sathe, C.; Butorin, S. M.; Shuh, D. K.; Nordgren, J.; Guo, J. One-Dimensional Quantum-Confinement Effect in  $\alpha$ -Fe<sub>2</sub>O<sub>3</sub> Ultrafine Nanorod Arrays. *Adv. Mater.* **2005**, *17*, 2320–2323.
- (8) Willets, K. A.; Van Duyne, R. P. Localized Surface Plasmon Resonance Spectroscopy and Sensing. *Annu. Rev. Phys. Chem.* **2007**, *58*, 267–297.
- (9) Huang, C.; Ye, J.; Wang, S.; Stakenborg, T.; Lagae, L. Gold Nanoring as a Sensitive Plasmonic Biosensor for On-Chip DNA Detection. *Appl. Phys. Lett.* **2012**, *100*, 173114.
- (10) Larsson, E. M.; Alegret, J.; Kall, M.; Sutherland, D. S. Sensing Characteristics of NIR Localized Surface Plasmon Resonances in Gold Nanorings for Application as Ultrasensitive Biosensors. *Nano Lett.* **2007**, *7*, 1256–1263.
- (11) Alu, A.; Engheta, N. Plasmonic and Metamaterial Cloaking: Physical Mechanisms and Potentials. *J. Opt. A: Pure Appl. Opt.* **2008**, *10*, 093002.
- (12) Cao, C.; Zhang, J.; Wen, X.; Dodson, S. L.; Dao, N. T.; Wong, L. M.; Wang, S.; Li, S.; Phan, A. T.; Xiong, Q. Metamaterials-Based Label-Free Nanosensor for Conformation and Affinity Biosensing. *ACS Nano* **2013**, *7*, 7583–7591.
- (13) Anker, J. N.; Hall, W. P.; Lyandres, O.; Shah, N. C.; Zhao, J.; Van Duyne, R. P. Biosensing with Plasmonic Nanosensors. *Nat. Mater.* **2008**, *7*, 442–453.
- (14) Wang, H.; Brandl, D. W.; Nordlander, P.; Halas, N. Plasmonic Nanostructures: Artificial Molecules. *Acc. Chem. Res.* **2007**, *40*, 53–62.
- (15) Liu, N.; Weiss, T.; Mesch, M.; Langguth, L.; Eigenthaler, U.; Hirscher, M.; Sonnichsen, C.; Giessen, H. Planar Metamaterial Analogue of Electromagnetically Induced Transparency for Plasmonic Sensing. *Nano Lett.* **2010**, *10*, 1103–1107.
- (16) Heyderman, L. J.; David, C.; Klaui, M.; Vaz, C. A. F.; Bland, J. Nanoscale Ferromagnetic Rings Fabricated by Electron-Beam Lithography. *J. Appl. Phys.* **2003**, *93*, 10011–10013.
- (17) Shelby, R. A.; Smith, D. R.; Schultz, S. Experimental Verification of a Negative Index of Refraction. *Science* **2001**, *292*, 77–79.
- (18) Linden, S.; Enkrich, C.; Wegener, M.; Zhou, J.; Koschny, T.; Soukoulis, C. M. Magnetic Response of Metamaterials at 100 Terahertz. *Science* **2004**, *306*, 1351–1353.
- (19) Bochenkov, V. E.; Sutherland, D. S. From Rings to Crescents: A Novel Fabrication Technique Unveils the Transition Details. *Nano Lett.* **2013**, *13*, 1216–1220.
- (20) Clark, A. W.; Glidle, A.; Cumming, D. R. S.; Cooper, J. M. Plasmonic Split-Ring Resonators as Dichroic Nanophotonic DNA Biosensors. *J. Am. Chem. Soc.* **2009**, *131*, 17615–17619.
- (21) Bukasov, R.; Ali, T. A.; Nordlander, P.; Shumaker-Parry, J. S. Probing the Plasmonic Near-Field of Gold Nanocrescent Antennas. *ACS Nano* **2010**, *4*, 6639–6650.
- (22) Bukasov, R.; Shumaker-Parry, J. S. Highly Tunable Infrared Extinction Properties of Gold Nanocrescents. *Nano Lett.* **2007**, *7*, 1113–1118.
- (23) Lewicka, Z. A.; Li, Y.; Bohloul, A.; Yu, W. W.; Colvin, V. L. Nanorings and Nanocrescents Formed via Shaped Nanosphere Lithography: A Route Toward Large Areas of Infrared Metamaterials. *Nanotechnology* **2013**, *24*, 115303–115313.
- (24) Cataldo, S.; Zhao, J.; Neubrech, F.; Frank, B.; Zhang, C.; Braun, P. V.; Giessen, H. Hole-Mask Colloidal Nano Lithography for Large-Area Low-Cost Metamaterials and Antenna-Assisted Surface-Enhanced Infrared Absorption Substrates. *ACS Nano* **2012**, *6*, 979–985.
- (25) Bukasov, R.; Shumaker-Parry, J. S. Silver Nanocrescents with Infrared Plasmonic Properties as Tunable Substrates for Surface Enhanced Infrared Absorption Spectroscopy. *Anal. Chem.* **2009**, *81*, 4531–4535.
- (26) Liu, G. L.; Lu, Y.; Kim, J.; Doll, J. C.; Lee, L. P. Magnetic Nanocrescents as Controllable Surface-Enhanced Raman Scattering Nanoprobes for Biomolecular Imaging. *Adv. Mater.* **2005**, *17*, 2683–2688.
- (27) Clark, A. W.; Sheridan, A. K.; Glidle, A.; Cumming, D. R. S.; Cooper, J. M. Tuneable Visible Resonances in Crescent Shaped Nano-Split-Ring Resonators. *Appl. Phys. Lett.* **2007**, *91*, 093109.
- (28) Rockstuhl, C.; Zentgraf, T.; Guo, H.; Liu, N.; Etrich, C.; Loa, I.; Syassen, K.; Kuhl, J.; Lederer, F.; Giessen, H. Resonances of Split-Ring Resonator Metamaterials in the Near Infrared. *Appl. Phys. B: Laser Opt.* **2006**, *84*, 219–227.
- (29) Pearson, D. H.; Tonucci, R. J. Nanochannel Glass Replica Membranes. *Science* **1995**, *270*, 68–70.
- (30) Pearson, D. H.; Tonucci, R. J. Parallel Patterning with Nanochannel Glass Replica Membranes. *Adv. Mater.* **1996**, *8*, 1031–1034.
- (31) Zhang, G.; Wang, D. Colloidal Lithography-The Art of Nanochemical Patterning. *Chem.—Asian J.* **2009**, *4*, 236–245.
- (32) Lusker, K. L.; Li, J. R.; Garino, J. C. Nanostructures of Functionalized Gold Nanoparticles Prepared by Particle Lithography with Organosilanes. *Langmuir* **2011**, *27*, 13269–13275.
- (33) Halpern, A. R.; Corn, R. M. Lithographically Patterned Electrodeposition of Gold, Silver, and Nickel Nanoring Arrays with Widely Tunable Near-Infrared Plasmonic Resonances. *ACS Nano* **2013**, *7*, 1755–1762.
- (34) Kumar, S.; Kumar, R.; Chakravarti, S. K. Morphological and Magnetic Characterization of Electrodeposited Cobalt Nanowires. *J. Mater. Sci.* **2004**, *39*, 2951–2953.
- (35) Loget, G.; Wood, J. B.; Cho, K.; Halpern, A. R.; Corn, R. M. Electrodeposition of Polydopamine Thin Films for DNA Patterning and Microarrays. *Anal. Chem.* **2013**, *85*, 9991–9995.
- (36) Sheridan, A. K.; Clark, A. W.; Glidle, A.; Cooper, J. M.; Cumming, D. R. S. Multiple Plasmon Resonances from Gold Nanostructures. *Appl. Phys. Lett.* **2007**, *90*, 143105.
- (37) Rockstuhl, C.; Lederer, F.; Etrich, C.; Zentgraf, T.; Kuhl, J.; Giessen, H. On the Reinterpretation of Resonances in Split-Ring-Resonators at Normal Incidence. *Opt. Express* **2006**, *14*, 8827–8836.
- (38) Gwinner, M. C.; Koroknay, E.; Fu, L.; Patoka, P.; Kandulski, W.; Giersig, M.; Giessen, H. Periodic Large-Area Metallic Split-Ring Resonator Metamaterial Fabrication Based on Shadow Nanosphere Lithography. *Small* **2009**, *5*, 400–406.

(39) Liu, S. D.; Zhang, Z. S.; Wang, Q. Q. High Sensitivity and Large Field Enhancement of Symmetry Broken Au Nanorings: Effect of Multipolar Plasmon Resonance and Propagation. *Opt. Express* **2009**, *17*, 2906–2917.

(40) He, K.; Smith, D. J.; McCartney, M. R. Direct Visualization of Three-Step Magnetization Reversal of Nanopatterned Spin-Valve Elements Using Off-Axis Electron Holography. *Appl. Phys. Lett.* **2009**, *94*, 172503.

(41) Madami, M.; Bisero, D.; Gubbiotti, G.; Tacchi, S.; Carlotti, G.; Nakano, K.; Ono, T. Magnetization Configurations in NiFe Slotted Rings Studied by Magneto-Optical Kerr Effect and Magnetic Force Microscopy. *IEEE Trans. Magn.* **2012**, *48*, 1269–1272.